Extent of low-grade Archaean metavolcanics in the northeastern Gawler Craton: new evidence and definition of the Devils Playground Volcanics

Anthony J Reid, Claire E Fricke and Wayne M Cowley *(Geological Survey Branch, PIRSA)*

Introduction

The bulk of the late Archaean volcanic–volcaniclastic rocks from the Gawler Craton range in age from c. 2535 to 2510 Ma (Fanning, Reid and Teale 2007). However, these units were preceded by an older set of volcanics, the c. 2558 calcalkaline volcanics of the northeastern Gawler Craton (Cowley and Fanning 1991). These older bimodal volcanics have not been discovered in outcrop and are confirmed only in one mineral exploration drillhole, DP1, located in the northern Olympic Cu–Au province, midway between Olympic Dam and Prominent Hill (Fig. 1). Upon discovery, these low-grade metavolcanics were initially correlated with the c. 1592 Ma Gawler Range Volcanics (Giles 1981). However, U–Pb zircon dating defined an eruption age of 2558 ± 6 Ma (Cowley and Fanning 1991) indicating the volcanics were a significantly older and unrelated magmatic event. These older volcanics, informally known as the Devils Playground Volcanics, are formally defined herein (see Appendix). The calcalkaline geochemistry and low-metamorphic grade make these volcanics an exploration target in themselves, with potential for volcanic-related sulfide and/or gold mineralisation.

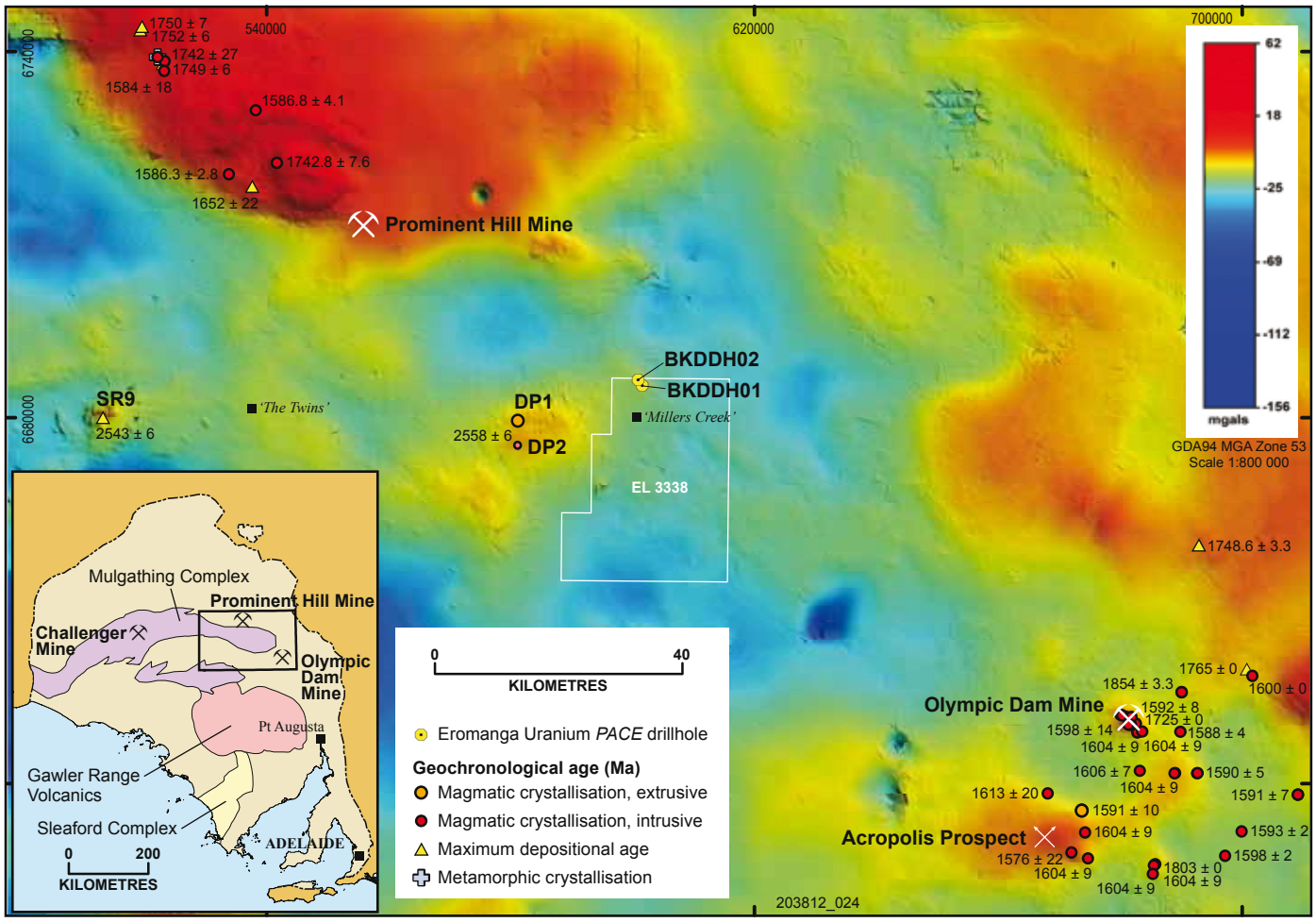

Figure 1 *Locality map of the northeastern Gawler Craton superimposed on a regional gravity dataset showing the Eromanga Uranium PACE-supported drillholes BKDDH01 and 02, related drillholes, mines, prospects, and regional geochronology (based on the compilation of Reid 2008). The ages are crystallisation ages in Ma. Map area is located in the Gawler Craton inset which shows the major Archaean to early Palaeoproterozoic domains and the Gawler Range Volcanics.*

Recent *PACE*-supported drilling by Eromanga Uranium Limited in the vicinity of DP1 intersected weakly metamorphosed basaltic to andesitic volcanics at depths <300 m. This article presents petrological and geochemical results from these recently discovered volcanics along with a discussion of possible correlations. The data has implications for our knowledge of the distribution, geochemistry and mineral potential of the c. 2558 Ma volcanism within the Gawler Craton.

Geological setting

Archaean to early Palaeoproterozoic rocks within the Gawler Craton are located within two regional belts, a northern belt known as the Mulgathing Complex and a southern belt known as the Sleaford Complex (Fig. 1). The oldest, c. 2558 Ma, volcanic rocks are found in the far eastern Mulgathing Complex, in the vicinity of Olympic Dam and Prominent Hill mines (Fig. 1). A wide variety of supracrustal rock types are preserved within the late Archaean to earliest Palaeoproterozoic rocks of the Gawler Craton, including felsic, mafic and ultramafic (komatiitic) volcanics, along with abundant chemical (banded iron formation) and clastic sediments (Daly and Fanning 1993). Generally, these rocks have undergone at least one major phase of deformation and have undergone greenschist to granulite facies metamorphism. Intruding into this Archaean supracrustal material are a series of early Palaeoproterozoic plutonic rocks that range in composition from peraluminous granitoids through to mantle-derived mafic and ultramafic gabbros and anorthosites.

Both the Mulgathing and Sleaford complexes are prospective for a range of commodities, principally gold, nickel and platinum group elements (PGE). Gold occurs within c. 2520 Ma granulite facies volcaniclastic rocks at the Challenger Mine (McFarlane, Mavrogenes and Tomkins 2007) and is present in a number of regional prospects across the western Mulgathing Complex (Birt and Reid 2007). Similar-aged ultramafic volcanics and komatiites occur within both the northern and southern belts and are prospective for nickel and PGE (Hoatson et al. 2005; Teale, Brewer and Lynch 2006). Earliest Palaeoproterozoic (c. 2440 Ma) ultramafic intrusives in the Mulgathing Complex also show evidence for Ni–Cu sulfide mineralisation (Daly and van der Stelt 1992; Daly and Fanning 1993).

The c. 2558 Ma Devils Playground Volcanics in drillhole DP1, from 166 m to total depth at 616.6 m, range from rhyodacite to andesite to basalt (Cowley and Fanning 1991). Geochemically these volcanics are calcalkaline and are isotopically moderately juvenile, with $\varepsilon Nd_{(2558\ Ma)}$ values that range from +2.3 to +3.1 (Cowley and Fanning 1991; Swain et al. 2005). The rocks are strongly sericite and chlorite altered and zones of quartz–sericite–chlorite ± carbonate schist are common within the DP1 core (Fig. 2a). The foliation is discontinuous at a scale of metres, with some zones showing no deformation fabric at all and thus retaining original volcanic features such as amygdales, feldspar phenocrysts and spherulites. As Cowley and Fanning (1991) reported, thin carbonate veining is common (Fig. 2b), while sulfides, principally pyrite, pyrrhotite and chalcopyrite, are sparse and sporadic. These features are important to bear in mind when considering the volcanics intersected in the recent Eromanga Uranium drilling. Depth to basement in the vicinity of DP1 is considerably variable, with a nearby drillhole, DP2 (Fig. 1), 4 km to the south, intersecting over 200 m of Phanerozoic cover, ~650 m of Pandurra Formation and no older units.

The relationship between the 'younger' c. 2535 to 2510 Ma volcanic–volcaniclastic sequences and the 'older' c. 2558 Ma Devils Playground Volcanics is uncertain, largely because the latter are known from only a single drillhole. Volcaniclastic rocks within both the Kenella Gneiss and informally named 'Challenger Gneiss' at Challenger Mine each preserve zircons with ages c. 2560 Ma (Swain et al. 2005; McFarlane, Mavrogenes and Tomkins 2007). This may indicate that detritus from the older sequences

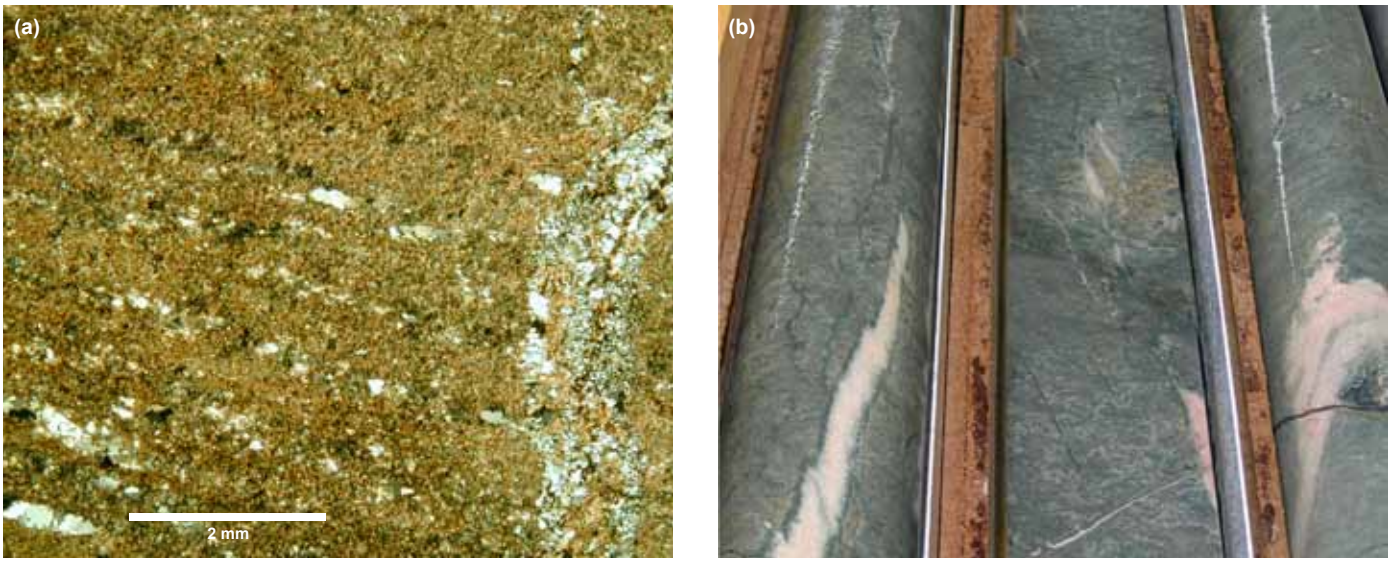

Figure 2 *Devils Playground Volcanics, DP1.* ***(a)*** *Photomicrograph of a schistose, sericitic metavolcanic, with recrystallised quartz lamellae defining a weak foliation. A narrow quartz–sericite vein truncates the layering.* ***(b)*** *Grey, weakly foliated metavolcanics, along with carbonate veining. (Photos 407728, 407707)*

was reworked into the younger sequences, possibly indicating localised exhumation of the older basin during deposition of the younger successions. Nevertheless, the structural relationship between the older and younger volcanic successions is obscured by younger cover.

Eromanga Uranium drilling: rationale and results

Eromanga Uranium's *PACE*-supported drilling program targeted iron oxide – copper–gold ± uranium mineralisation through identification of a near-coincident gravity and magnetic anomaly along a NW-trending gravity ridge (within Exploration Licence 3338; Fig. 1). Three peak gravity responses and a small, circular magnetic anomaly are located along the ridge. Geophysical modelling of the gravity and magnetic data indicated basement was likely located ~300 m below Permian to Tertiary cover. Two diamond drillholes were planned to test the geophysical anomalies, BKDDH01 and BKDDH02 (Fig. 1).

Both drillholes intersected a similar cover sequence comprising Tertiary Millers Creek Dolomite and Billa Kalina Clay members of the Mirikata Formation, the Cretaceous Cadna-owie Formation and the Permian Boorthanna Formation (Fig. 3). These units lie unconformably over the basement rocks. The basement intersected in both holes comprises metamorphosed, pyroxene–plagioclase basalts and minor andesites (Fig. 3), which we will refer to generically as the 'BKDDH01 and 02 basalts' hereafter.

The BKDDH01 and 02 basalts are weakly to strongly overprinted by an actinolite–albite–chlorite–epidote–carbonate–titanite alteration assemblage (Figs 4a, b). Major portions of the metabasalt show fragmentation textures (Fig. 4c), flow brecciation and minor tuffs. Persistent quartz and carbonate veining, containing chlorite, epidote, adularia and rare pyrite, occurs throughout (Figs 4d, e). Penetrative tectonic fabrics are interpreted to be present within the sequence, with some intervals of tremolite–chlorite–quartz–albite schist suggesting localisation of deformation and concomitant recrystallisation into zones <20 m thick (Figs 3, 4e, f). Quartz and carbonate veining appears to be coeval with chloritic alteration (Fig. 4f), indicating a broadly greenschist, ~250–400 °C temperature window for the alteration and deformation event.

Geochemical and isotopic features of BKDDH01 and 02 basalts

Major and trace element geochemistry were determined for 13 samples of metabasalt from BKDDH01 and 02 by Australian Laboratory Services Pty Ltd. Major elements were determined by lithium metaborate fusion, followed by inductively coupled plasma - atomic emission spectroscopy (ICP-AES). Trace and rare earth elements (REE) were determined by lithium borate fusion followed by ICP - mass spectroscopy (ICP-MS). Volatiles (As, Bi, Hg, Sb, Se, Te) were determined through aqua regia solution followed by ICP-MS. Geochemical results for the samples are presented in Table 1.

Sm and Nd isotopic compositions of two metabasalt samples were obtained at the University of Adelaide following the methods of Wade, Barovich and Hand (2006). Whole-rock samples were spiked with a ^{150}Nd–^{147}Sm solution and dissolved in hydrofluoric acid at 190 °C for five days in sealed Teflon bombs. Nd and Sm concentrations were calculated by isotope dilution, with Nd isotope ratios measured by thermal ionisation mass spectrometry on a Finnigan MAT 262 mass spectrometer, and Sm isotope ratios measured on a Finnigan MAT 261 mass spectrometer. The long-term average for $^{143}Nd/^{144}Nd$ of the La Jolla standard for the year to the date of the present analyses is 0.51183 (n = 111).

Compositionally the BKDDH01 and 02 samples range from basalt to andesite (Fig. 5) and have SiO_2 values between 50% and 60% (Table 1). Major oxide composition decreases with increasing SiO_2, particularly Fe_2O_3 and MgO (Fig. 6). The Na_2O value for the samples does not appear to show any trend with changing SiO_2, possibly a result of alteration. Trace element values are generally negatively correlated with SiO_2, such that lower silica compositions typically yield higher Ni, Nb and Cr values (Fig. 6). Such variation is typical of the differentiation trend expected for comagmatic volcanics.

Trace element data displays an overall trend of a higher large ion lithophile element composition, which contrasts with the low values for the high-field strength elements (Fig. 7a). The trace element data also reveals strong Nb, Ta and Ti depletions, and a moderate depletion in P. These depletions are strikingly similar to an average value for trace elements derived from a large database of analyses from subducted sediment (Plank and Langmuir 1998). Interestingly, we note that the low Y (<20 ppm) and large range of Cr values (290–1270 ppm) for these samples is very similar to the ranges found in volcanic arc basalts (Pearce 1982). Furthermore, the BKDDH01 and 02 samples are enriched in light REE (LREE), with an average chondrite-normalised La_N/Yb_N value of 8.3. The magnitude of enrichment in the LREE is comparable to a bulk crustal composition, and likewise to an average global subducted sediment composition (Fig. 7). In contrast, the heavy REE (HREE) are not enriched, being comparable to depleted mantle values. The samples generally show a weak or no negative Eu anomaly, with Eu/Eu* values ≤1.0, indicating little or no plagioclase fractionation from these melts.

This data indicates that these magmas were likely derived from mantle material that either incorporated crustal material during magma ascent, or that the mantle source itself was enriched in the large ion lithophile elements and LREE. If volcanic arc processes were responsible for formation of these magmas, then enrichment in these elements may be a result of incorporation of these elements into the mantle wedge via subduction of sedimentary material.

Measured $^{143}Nd/^{144}Nd$ values for the two samples are 0.511491 and 0.511451, with corresponding present day εNd values around –22 (Table 2). Depleted mantle model ages for the samples are 3.28 and 3.18 Ga. The isotopic data suggests that the basaltic material is contaminated by crustal material with a prehistory extending back to c. 3.2 Ga.

	From	To	Interval (m)	Age	Formation	Description
	0	6	6.0	Tertiary	Millers Creek Dolomite Member	Cream to white dolomite, dolomitic limestone
	6	16	10.0	Tertiary	Billa Kalina Clay Member	Green clay, minor quartz grains
	16	34	18.0	Cretaceous	Cadna-owie Formation	Feldspathic sandstone
	34	317.2	283.2	Permian	Boorthanna Formation	Glacial mudstone, fine sandy mudstone and fine sandstone
Unconformity	317.2	341	23.8	? Archaean		Metamorphosed porphyritic basalt, common high-angle carbonate veins to 10 mm wide infill breccia common hematite stringers and veins
	341	360	19.0			Metamorphosed porphyritic basalt sheared in places
	360	362.6	2.6			Flow brecciated, metamorphosed porphyritic basalt, albite rimmed/altered basalt fragments, basaltic andesite
	362.6	366.2	4.0			Metamorphosed porphyritic basalt
	366.2	366.5	0.3			Porphyritic andesite lava
	366.5	373.5	7.0			Metamorphosed porphyritic basalt, Si altered
	373.5	376.1	2.6			Metamorphosed porphyritic basalt, moderately foliated/sheared
	376.1	396	19.9			Metamorphosed porphyritic basalt
	396	403	7.0			Metamorphosed porphyritic basalt, moderately foliated/sheared, basalt/ultramafic
	403	414	11.0			Fragmental/brecciated metamorphosed porphyritic basalt
	414	425.6	11.6			Metamorphosed porphyritic basalt, network of fine hem. veins
	425.6	432	6.4			Fragmental metamorphosed porphyritic basalt, strongly foliated and qtz veined
	432	444.8	12.8			Brecciated metamorphosed porphyritic basalt, lapilli tuff?
	444.8	456.2	11.4			Metamorphosed porphyritic andesite lava, zoned phenocrysts, common qtz hem./albite veining
	456.2	468.2	12.0			Fragmented, flow-brecciated, metamorphosed porhyritic basalt, minor qtz, carb., hem. veins <3 mm
	468.2	476.6	8.4			Metamorphosed porphyritic metabasalt, stong foliation at 45 deg to CA, qtz carb. veining throughout
	476.6	534	57.4			Metamorphosed porphyritic basalt
	534	548.7	14.7			Metamorphosed finer grained porphyritic basalt
	548.7	563.2	14.5			Foliated, fine-grained, metamorphosed porphyritic metabasalt, minor basaltic lapilli tuff
	563.2	564.4	1.2			Porphyritic andesite
	564.4	575.7	11.3			Metamorphosed porphyritic basalt
	575.7	588	12.3			Metamorphosed dacite/andesite lava
	588	595.7	7.7			Metamorphosed porphyritic basalt

Figure 3 *Geological log of BKDDH02 by Eromanga Uranium. Depth to basement is around 317 m. BKDDH01's geological log is very similar.*

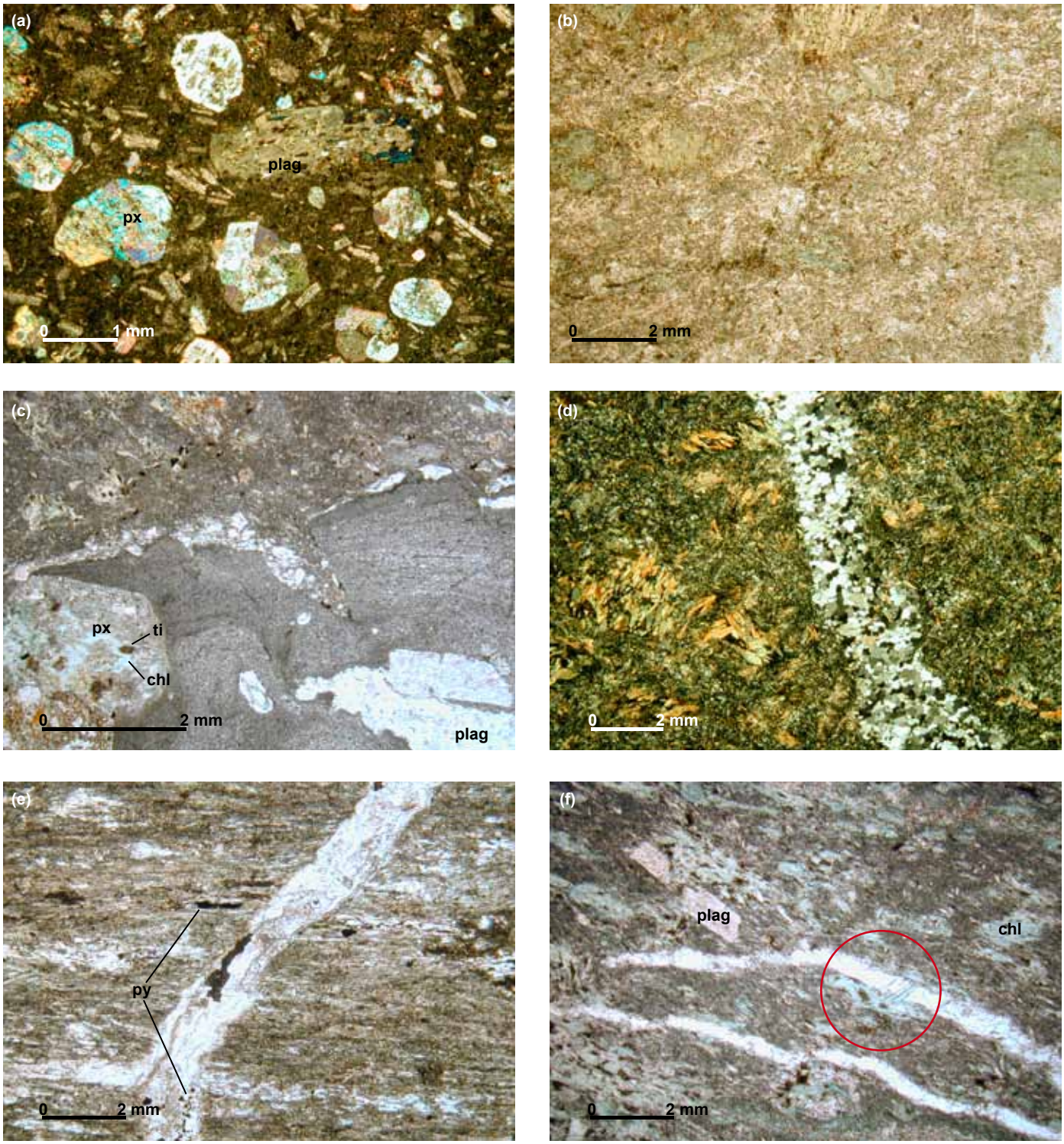

Figure 4 *Photomicrographs of rock types from BKDDH02.* ***(a)*** *Relatively unaltered basalt, with coarse pyroxene (px) and plagioclase (plag) phenocrysts within a fine-grained, sericite–actinolite matrix. Both species of phenocrysts are variably altered, with the large plagioclase grain in the centre of the field of view showing coarse actinolite (blue birefringence) and local chlorite overgrowths. Crossed nicols, 361.4 m.* ***(b)*** *Metamorphosed basalt with aggregates of actinolite + hornblende ± chlorite (green) pseudomorphing pyroxene phenocrysts or possibly replacing amygdales. Groundmass comprises fine-grained albite, actinolite, biotite, carbonate, epidote and titanite. Plain light, 349.1 m.* ***(c)*** *Fragmentation texture in thin section, with the lower, presumably older, lava showing flow banding parallel to the flow margin along with coarse-plagioclase and pyroxene phenocrysts, the latter partially replaced by titanite (ti) and chlorite (chl). The surface of the lava has fractured and is infilled by the upper, presumably younger, lava flow. The upper lava shows a coarser grained, opaque-bearing groundmass, now recrystallised to actinolite–chlorite ± sericite and finer grained phenocrysts that are now completely replaced by actinolite + hornblende ± chlorite. The fragmentation may have occurred as a result of cooling of the lava following eruption. Note that a quartz-rich alteration band appears to have preferentially sited at the boundary between the two flows. Crossed nicols, 456.2 m.* ***(d)*** *Quartz vein comprising granular quartz, with minor chlorite ± actinolite intruding metabasalt. Crossed nicols, 349.1 m.* ***(e)*** *Foliated tremolite–chlorite–quartz/albite schist. Pyrite (py), titanite and opaque oxide occur within the foliation. A carbonate–quartz vein crosscuts the foliation and contains pyrite, chlorite and minor adularia. Plain light, 399.7 m.* ***(f)*** *Weakly foliated metabasalt, with abundant chlorite alteration. Two narrow carbonate veins truncate the foliation and are also intergrown with chlorite (circled), indicating pervasive alteration post-dates at least some carbonate veining. Plain light, 534.3 m. (Photos 407729–407734)*

Table 1 *Whole rock geochemical data for samples from BKDDH01 and 02*

SAMPLE	10726	10671	10675	10728	10673	10672	10729	10676	10674	10677	10724	10725	10727
BKDDH	01	02	02	01	02	02	01	02	02	02	01	01	01
Depth (m)	330.2	353.2	534.3	371	449.2	381.2	455.2	564	454.6	585.8	280.8	328.4	345.8
Classification	Basalt	B-and.	B-and.	B-and.	B-and.	B-and.	B-and.	B-and.	Andesite	T-and.	Andesite	Andesite	Andesite
SiO_2	51	52.4	52.8	53	53.3	53.5	53.6	54.3	55.7	56.5	57.6	59.1	59.3
Al_2O_3	11.6	12.7	13.45	12.95	14.95	13.4	14.5	14.6	14.3	16.95	10.45	13.6	14.55
Fe_2O_3	10.15	9.27	9.05	8.11	8.48	8.13	7.93	7.58	7.41	5.43	8.11	6.02	6.24
CaO	5.67	8.56	6.11	8.26	7.75	8.3	9.85	7.09	7	5.87	6.45	4.04	5.18
MgO	12.5	9.72	9.21	10.45	8.32	8.86	4.05	8.03	8	4.32	10.1	6.19	6.17
Na_2O	0.87	2.64	3.19	2.11	2.71	2.76	2.11	3.09	2.91	5.98	1.73	2.85	3.96
K_2O	1.76	1.17	1.51	1.3	0.93	1.02	1.56	1.42	1.25	1.09	0.94	1.27	1.23
Cr_2O_3	0.16	0.09	0.12	0.13	0.06	0.09	0.04	0.07	0.06	0.04	0.13	0.04	0.05
TiO_2	0.6	0.71	0.61	0.53	0.67	0.77	0.68	0.54	0.58	0.55	0.51	0.46	0.51
MnO	0.21	0.18	0.16	0.14	0.15	0.15	0.21	0.13	0.11	0.08	0.13	0.11	0.12
P_2O_5	0.09	0.17	0.15	0.15	0.1	0.16	0.13	0.09	0.09	0.1	0.09	0.12	0.11
SrO	0.02	0.06	0.04	0.05	0.06	0.08	0.07	0.09	0.06	0.04	0.04	0.05	0.05
BaO	0.13	0.07	0.1	0.08	0.03	0.07	0.06	0.05	0.06	0.08	0.05	0.07	0.05
LOI	5.6	1.97	3.03	2.4	2.42	2.31	5.13	2.68	2.25	2.91	2.52	3.6	NSS
Total	100.36	99.71	99.53	99.66	99.93	99.6	99.92	99.76	99.78	99.94	98.85	97.52	97.52
C	0.2	0.04	0.11	0.04	0.04	0.11	0.86	0.17	0.04	0.41	0.04	0.08	0.06
S	0.01	0.01	0.01	0.01	0.01	0.02	0.25	<0.01	0.02	0.01	0.02	0.07	0.01
Ag	<1	<1	<1	<1	<1	<1	<1	<1	<1	<1	<1	<1	<1
Ba	1005	656	909	731	302	598	556	420	509	736	392	549	393
Ce	32.1	54.3	46.4	36	23.5	53.1	36.1	19.8	28.8	27.8	30.7	24.3	31.1
Co	55	41.3	42.2	47.7	38.6	48.4	30.5	36.4	44.2	36.7	53.2	29.5	31.9
Cr	1270	650	920	1000	430	660	290	470	460	320	900	330	360
Cs	0.61	1.76	1.43	2.51	1.32	1.78	3.58	4.12	1.28	1.32	1.58	1.38	2.57
Cu	82	12	26	35	45	45	68	29	52	42	43	62	44
Dy	2.39	3.34	2.85	2.54	2.87	3.4	3.2	2.24	2.49	2.29	1.85	1.65	2.03
Er	1.43	2	1.69	1.48	1.74	1.95	1.87	1.33	1.48	1.31	1.17	1.07	1.28
Eu	1.02	1.55	1.42	1.03	1.02	1.52	1.28	0.79	0.97	0.96	0.54	0.66	0.71
Ga	15	20.6	19	17	18.7	18.7	19.9	17.1	19.1	18.8	12.4	16.1	17.7
Gd	3.52	4.62	4.08	3.31	3.23	4.73	3.95	2.51	3.03	2.89	2.65	2.41	2.79
Hf	2.7	3	3	2.6	2.6	3.1	3	2.3	2.8	3.1	2	2.5	3.5
Ho	0.54	0.62	0.54	0.47	0.57	0.63	0.61	0.43	0.46	0.44	0.43	0.38	0.46
La	14	27.2	23.7	17.7	11.4	25.6	17.9	9.8	14.7	14.1	14.5	11.8	14.2
Lu	0.21	0.25	0.22	0.22	0.25	0.25	0.27	0.19	0.21	0.17	0.18	0.16	0.18
Mo	<2	16	<2	<2	3	2	<2	<2	<2	<2	<2	<2	<2
Nb	3.9	4.7	3.8	3.9	3.2	4.5	4.1	2.7	3.5	3.6	3.6	3.1	3.7
Nd	13.9	30.1	26	18.4	14.2	30.3	19.8	11.4	15.6	15	12.5	10.2	13
Ni	335	169	302	275	153	164	75	168	159	118	266	117	126
Pb	33	21	11	18	12	17	31	12	10	7	745	16	21
Pr	3.85	7.47	6.17	4.56	3.24	7.25	4.84	2.71	3.83	3.64	3.66	2.98	3.66
Rb	52	33.1	34.2	36	28	28.2	52	51.9	36	28.3	26.9	43.6	45.2
Sm	3.14	5.37	4.72	3.4	3.05	5.38	3.94	2.48	3.13	2.83	2.52	2.23	2.68
Sn	2	1	1	1	1	1	1	1	1	1	2	3	3
Sr	178.5	475	339	452	478	645	575	686	501	386	279	388	392
Ta	0.2	0.4	0.3	0.3	0.3	0.3	0.3	0.2	0.2	0.3	0.2	0.2	0.3
Tb	0.51	0.61	0.53	0.46	0.47	0.61	0.56	0.36	0.42	0.4	0.38	0.35	0.42
Th	4	5.42	4.9	4.39	2.42	5.26	3.7	2.16	2.75	3.21	4.01	3.04	3.94
Tl	<0.5	<0.5	<0.5	<0.5	<0.5	<0.5	<0.5	<0.5	<0.5	<0.5	<0.5	<0.5	<0.5
Tm	0.22	0.25	0.22	0.2	0.24	0.26	0.25	0.18	0.2	0.17	0.18	0.17	0.21
U	0.86	1.2	1.09	1.63	0.61	1.16	0.91	0.51	0.65	0.83	0.81	0.83	0.96
V	176	174	146	140	151	168	175	127	140	104	149	129	142
W	2	4	4	5	5	2	3	2	2	1	2	2	2
Y	12.9	17.9	15.4	13.3	15.2	17.2	16.8	11.9	13.3	11.7	9.6	9.1	10.9
Yb	1.32	1.74	1.41	1.37	1.64	1.79	1.73	1.24	1.33	1.16	1.05	0.92	1.11
Zn	119	109	95	98	70	109	172	70	129	43	106	74	79
Zr	109	104	106	92	92	107	102	81	101	110	79	97	144
As	6	29.8	11.5	6	43.6	67.1	7.7	12.5	83.9	24.2	25.2	8.7	20.2
Bi	0.08	0.16	0.11	0.08	0.07	0.07	0.09	0.08	0.07	0.08	0.14	0.08	0.11
Hg	0.006	0.007	0.008	0.006	0.005	0.006	0.02	<0.005	<0.005	0.008	0.006	0.005	<0.005
Sb	1.02	3.92	5.44	1.93	5.55	4.9	3.78	5.29	13.05	3.97	1.86	18.6	3.17
Se	0.4	0.4	0.3	0.4	0.3	0.3	0.5	0.3	0.3	0.3	0.4	0.3	0.4
Te	<0.01	<0.01	0.01	0.01	0.01	0.01	0.01	<0.01	0.01	0.02	0.01	0.01	0.01
La_N/Yb_N	7.2	10.6	11.4	8.8	4.7	9.7	7.0	5.4	7.5	8.3	9.4	8.7	8.7
Eu/Eu*	0.9	0.9	1.0	0.9	1.0	0.9	1.0	1.0	1.0	1.0	0.6	0.9	0.8

Notes: NSS = not sufficient sample. Classification is from total alkali vs silica diagram. B-and. = basaltic andesite. T-and. = trachyandesite.

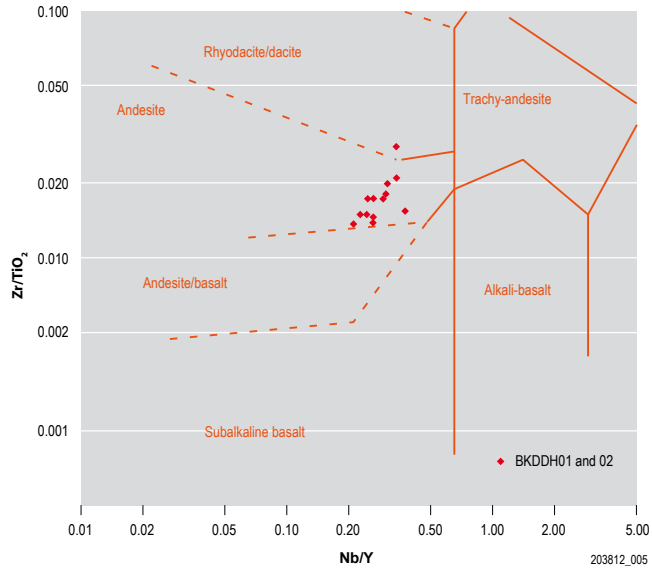

Figure 5 *Nb/Y–Zr/TiO_2 classification diagram (Winchester and Floyd 1977) for samples from BKDDH01 and 02. This and other geochemical diagrams in this paper were constructed using GCDKit 2.3 (Janoušek et al. 2006).*

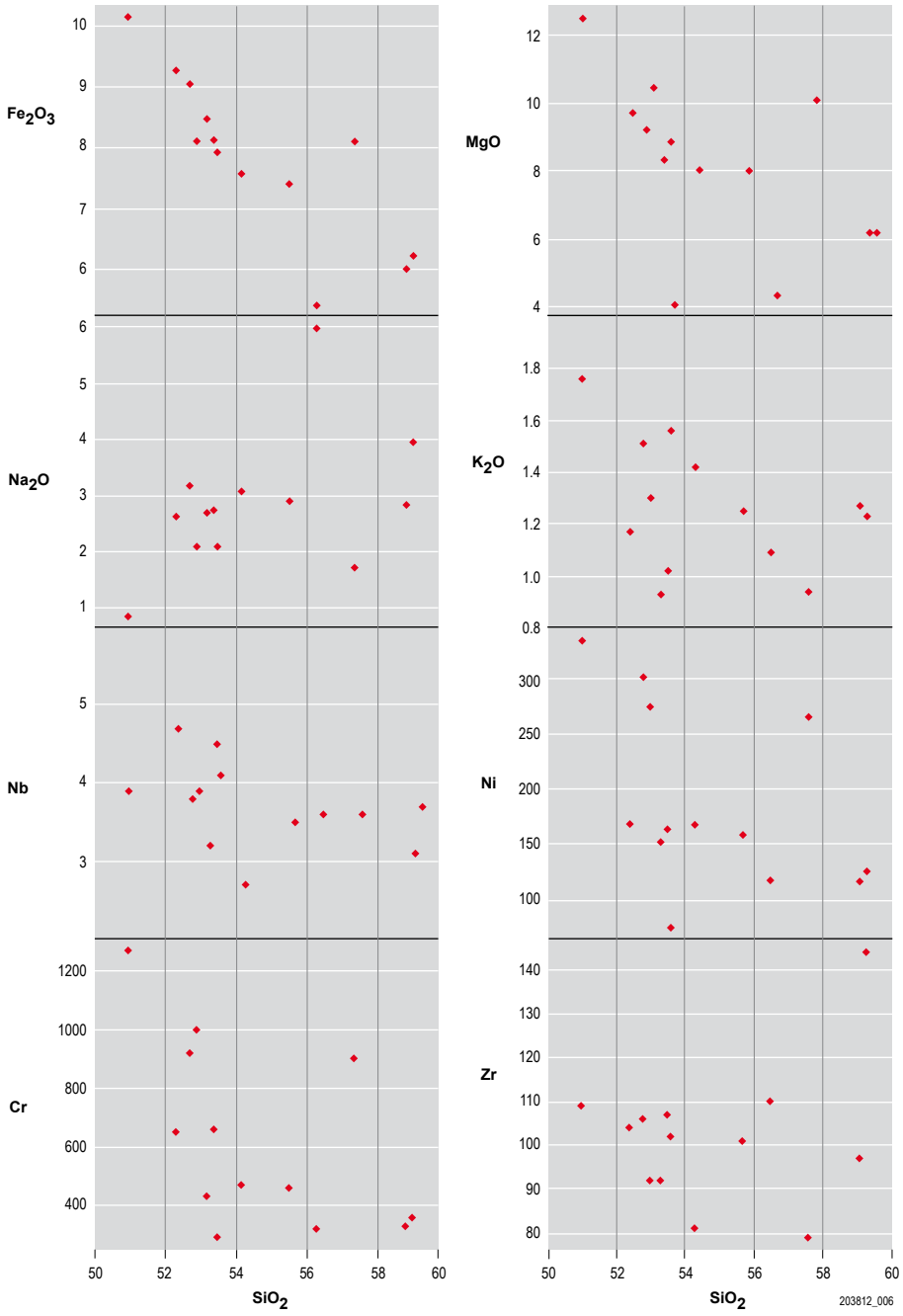

Figure 6 *Harker variation diagrams for selected major and trace elements for samples from BKDDH01 and 02.*

Possible geochemical correlations

In this section we present a comparison of the data from the BKDDH01 and 02 basalts with three possible correlatives that comprise low-metamorphic grade and little-deformed volcanic units: (i) Archaean Devils Playground Volcanics basalt from DP1; (ii) examples of South Australian Mesoproterozoic basalt from the Gawler Range Volcanics; and (iii) Mesoproterozoic Benagerie Volcanics of the Curnamona Province in the central eastern part of South Australia, east of the Gawler Craton. When plotted together with all available samples from drillhole DP1, the BKDDH01 and 02 samples appear to define similar trends in terms of their incompatible element composition, in particular Zr and TiO_2 (Figs 8a, b). The Mesoproterozoic basalts of the Gawler Range Volcanics have similar Zr abundances, but are distinctly elevated in TiO_2 in comparison with either the BKDDH01 and 02 basalts or those of DP1 (Fig. 8a). Likewise, basalts of the Benagerie Volcanics are distinctly elevated in both Zr and TiO_2 and are therefore not likely to be correlatives.

Figure 9 shows a comparison between the REE values for metabasalt from BKDDH01 and 02 and those of three possible correlatives. In each case, only samples with SiO_2 <60% have been used for the comparison. Basalt from DP1 shows very similar trends to the field for the BKDDH01 and 02 samples, with LREE enrichment and little or no enrichment in HREE. In contrast, the Gawler Range Volcanics basalts are enriched in all REE, a distinction that is particularly important in terms of the HREE. Benagerie Volcanics from drillhole LNM10 show a much flatter REE profile, with considerably less LREE enrichment and elevated HREE values compared to the samples from BKDDH01 and 02. This data suggests that it is much more likely that the basalts in BKDDH01 and 02 are correlatives of the Devils Playground Volcanics basalts in DP1 rather than part of the Mesoproterozoic Gawler Range or Benagerie volcanics.

Table 2 *Sm–Nd isotopic data for samples from BKDDH01*

Sample	Source	Age (Ga)	Nd (ppm)	Sm (ppm)	$^{147}Sm/^{144}Nd$	$^{143}Nd/^{144}Nd$	2σ	εNd_0	εNd_i	TDM (Ga)
1667143	BKDDH01, 416.8–420.0 m	2.553	13.9	3.14	0.136646	0.511533	10	–21.6	–1.9	3.20
1667144	BKDDH01, 327.5–327.0 m	2.553	10.2	2.23	0.132248	0.511502	10	–22.2	–1.0	3.08

Notes: $^{143}Nd/^{144}Nd$ CHUR(0) = 0.512638. $^{147}Sm/^{144}Nd$ CHUR = 0.1966. $^{143}Nd/^{144}Nd$ DM(0) = 0.51235. $^{147}Sm/^{144}Nd$ DM = 0.2137.

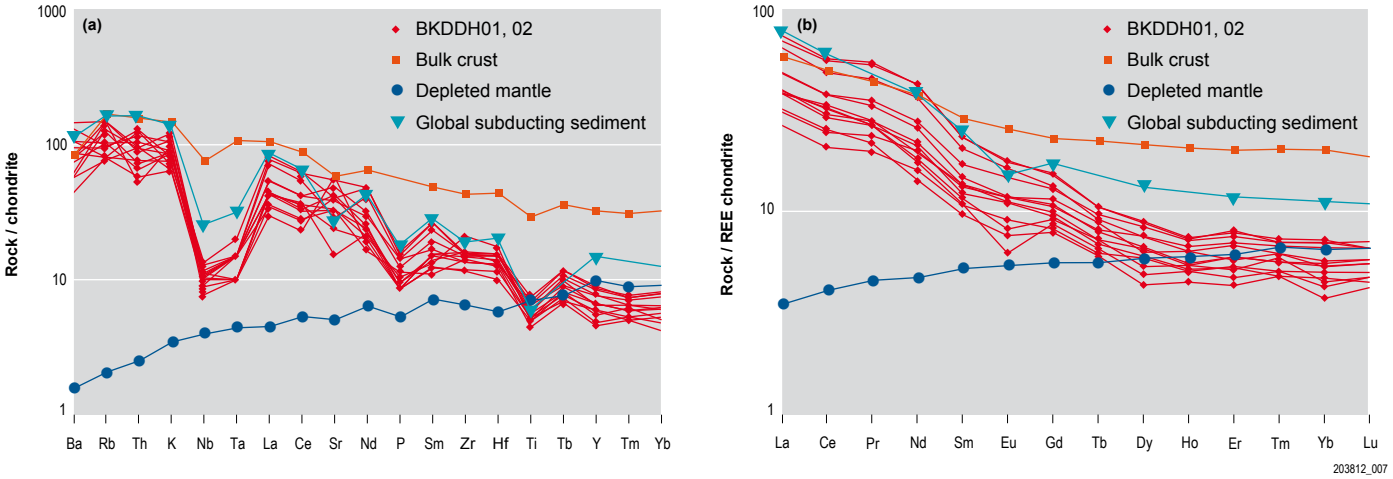

Figure 7 *Trace and REE diagram for samples from BKDDH01 and 02.* ***(a)*** *Chondrite-normalised REE plot (normalising values of Thompson 1982).* ***(b)*** *Chondrite-normalised trace element plot (normalising values of Taylor and McLennan 1985). Shown for reference are values for the bulk crust (Taylor and McLennan 1985), depleted mantle (Salters and Stracke 2004) and global subducted sediment (GLOSS; Plank and Langmiur 1998) reservoirs.*

In detail, we note that at comparable low SiO_2 compositions, the Devils Playground Volcanics from DP1 are slightly elevated in Zr and Ti, beyond the BKDDH01 and 02 basalts (Figs 8a, b). If this elevation in the DP1 samples was due to greater fractional crystallisation from a similar source to the BKDDH01 and 02 basalts, then this would impact on the REE profiles for DP1 such that the LREE would be expected to be steeper and less elevated, with the converse for the HREE. However, the REE profiles for both DP1 and BKDDH01 and 02 basalts are similar in both magnitude and form (Fig. 9). This suggests that these two sets of volcanics are unlikely to have resulted from an identical magma batch, rather, that similar variable degrees of assimilation processes were operating during formation of these volcanics. Since we envisage either crustal contamination or input of subducted material into the formation of both DP1 volcanics and the BKDDH01 and 02 basalts, minor variation in such trace element abundances are perhaps not surprising.

Sm–Nd isotopic data provides further evidence for the likely correlation between the basalts in BKDDH01 and 02 and those in DP1. Figure 10 shows the εNd data plotted against time for BKDDH01 samples along with those of DP1 and mafic Gawler Range Volcanics. The plot demonstrates that the BKDDH01 samples are too evolved to lie within the field defined by the mafic Gawler Range Volcanics. Conversely, the εNd values for the DP1 samples plot directly over the field defined for the BKDDH01 samples.

Interestingly, a Jensen plot (Mg–Fe + Ti–Al: Fig. 11) of the DP1 and BKDDH01 and 02 basalts forms an apparent geochemical trend that ranges from komatiitic basalt, through high-Mg basalt to the calcalkaline dacite preserved only in DP1. Such a trend would be expected for a series of broadly contemporaneous volcanics that resulted from variable assimilation and fractional crystallisation processes to produce melts of different composition. If this correlation between the BKDDH01 and 02 basalts and the bimodal volcanics found in DP1 is accepted, then this extends the known low-grade Archaean province of the northeastern Gawler Craton some distance to the northeast of DP1.

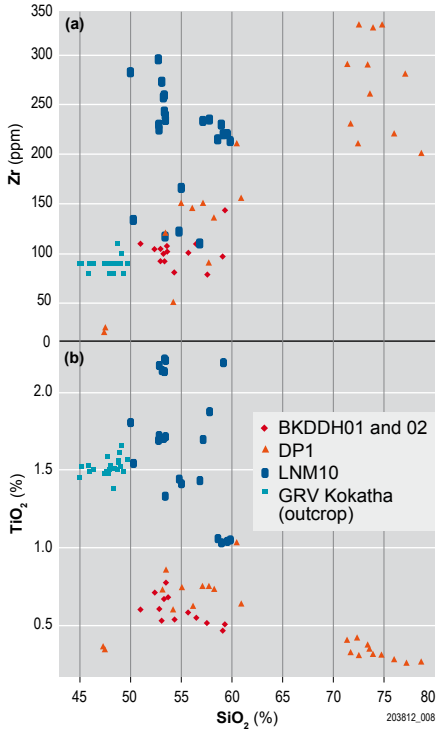

Figure 8 *Apparent geochemical similarities defined by pooling data for BKDDH01 and 02 with data from DP1. DP1 data from Swain et al. (2005) and Cowley and Fanning (1991). Also shown for comparison are corresponding data from the Gawler Range Volcanics (Fricke 2005) and Benagerie Volcanics, LMN10 (PIRSA, unpublished data, 2008).* ***(a)*** *SiO_2 versus Zr.* ***(b)*** *SiO_2 versus TiO_2.*

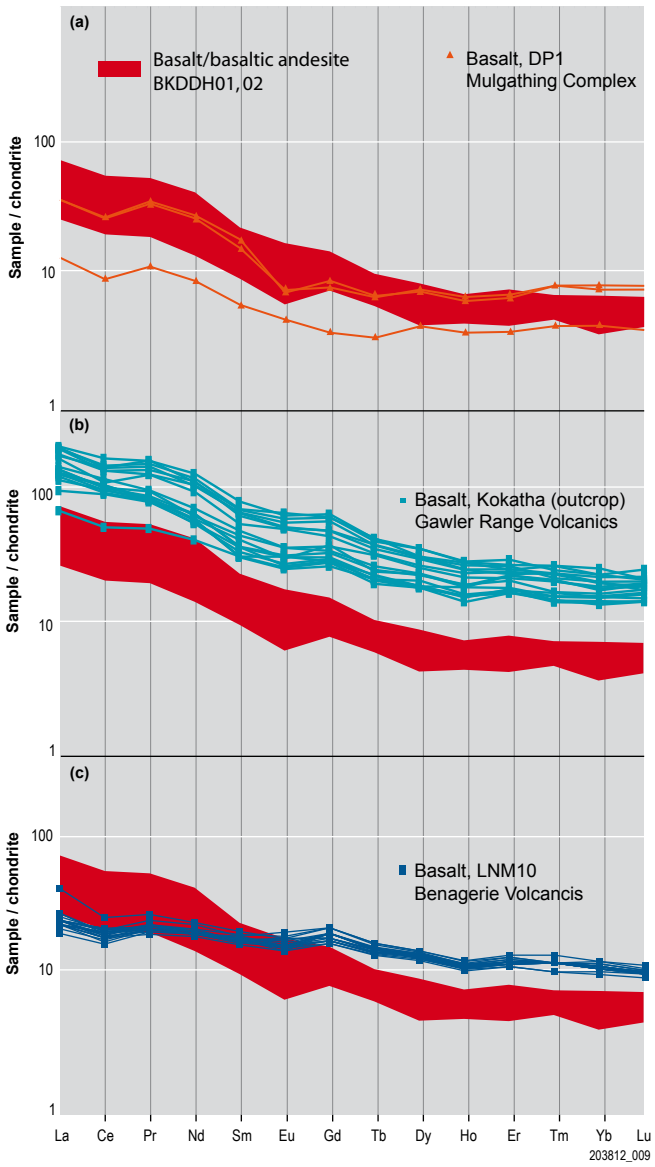

Figure 9 *Chondrite-normalised REE diagram comparing three possible correlatives with metabasalts from BKDDH01 and 02.* ***(a)*** *DP1 (data from Swain et al. 2005) and BKDDH01 and 02.* ***(b)*** *Gawler Range Volcanics (data from Fricke 2005).* ***(c)*** *Benagerie Volcanics (unpublished data from PIRSA 2008). Normalising values from Thompson (1982).*

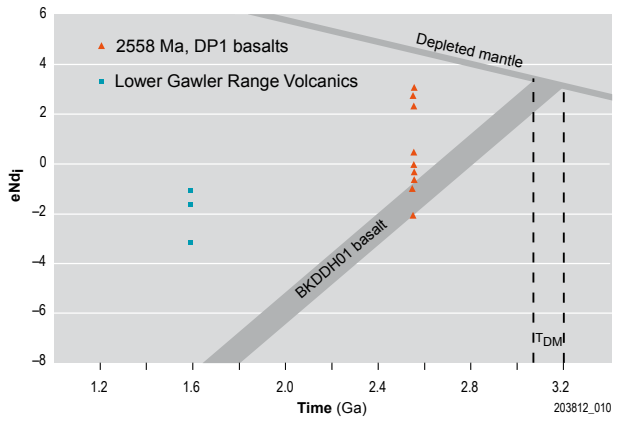

Figure 10 *εNd evolution diagram showing samples from BKDDH01, DP1 and lower Gawler Range Volcanics compared to depleted mantle. Comparison data from Cowley and Fanning (1991) and Fricke (2005).*

Discussion and conclusion

The volcanics intersected in BKDDH01 and 02 include high-Mg basalts transitional to komatiitic basalts, along with calcalkaline andesites. The high Mg content, together with the enrichment in LREE and significant depletions in Nb, Ta and Ti suggest that either these mantle-derived melts underwent significant crustal contamination during ascent through the crust or that the mantle source was enriched in a variable source, such as may be provided by the input of subducted sediment in a convergent margin setting. The prehistory of the crustal material within these basalts extends to c. 3.2 Ga.

A correlation between the BKDDH01 and 02 basalts and the more fractionated DP1 Devils Playground Volcanics is proposed based largely on similarity in both trace element compositions for samples with similar SiO_2 values and Sm–Nd isotopic values. It is also important to note the comparable low metamorphic grade and greenschist facies alteration assemblages found in both the DP1 volcanics and the BKDDH01 and 02 basalts. The similar carbonate veining and sericite–chloritic alteration strongly suggest that the two volcanic successions have undergone similar post-eruptive metamorphic/alteration history. We also note that in drillhole SR9, Jagodzinski (2005) has documented arenaceous sandstone containing dacitic rock fragments which yielded a maximum depositional age of 2543 ± 6 Ma (SHRIMP zircon U–Pb; see Fig. 1 for location). These sediments have undergone a similar low-grade regional metamorphism with albite, sericite, chlorite and calcite alteration. The source for this sediment was interpreted by Jagodzinski (2005) to be local and it is possible that this indicates that the low-grade Archaean metavolcanic province extends at least this far west. Further work in this region will undoubtedly yield more information on the lateral extent of this province and the relationship between these apparently slightly younger dacitic lavas preserved as fragments in SR9.

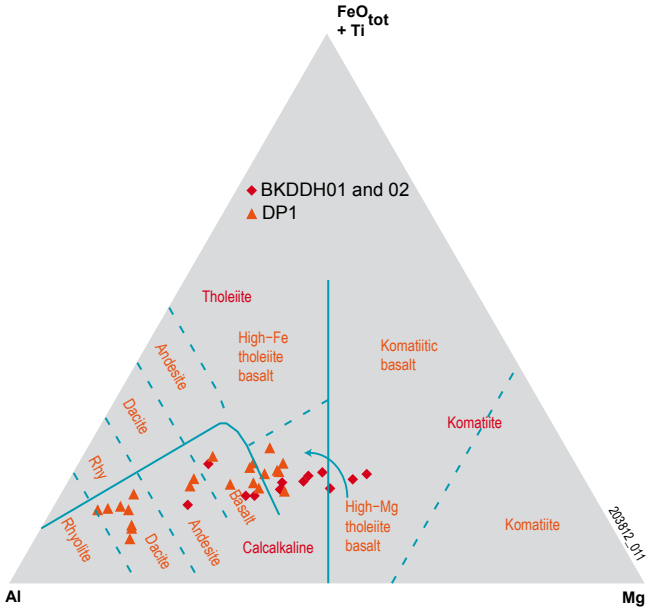

Figure 11 *Fe–Al–Mg cation plot for classifying subalkaline volcanic rocks (Jensen 1976) for the samples from BKDDH01, 02 and DP1.*

These correlations likely extend the c. 2558 Ma volcanic province of the northeastern Gawler Craton and have implications for exploration models in this region. The potentially plate margin Devils Playground Volcanics are prospective for base metal sulfides and gold, however, suitable hydrothermal systems would be required to concentrate the metals present within these volcanics. The presence of low-temperature quartz and carbonate veining during metamorphism and deformation suggests temperatures within the rock mass may have been suitable for these systems to have developed. Of particular importance for future exploration work will be to identify the location of basement highs, since the thick cover of Pandurra Formation along with younger sediment in this region obscures the basement over large areas (Cowley and Martin 1991). Seismic and also gravity data would potentially be helpful in defining the depth to basement in this regard. Based on a depth-to-basement model, targeting of structural settings (traps) identified in magnetic data is likely to be the principal method if future exploration is to be attempted in this low-grade, likely late Archaean volcanic province.

Appendix: definition of Devils Playground Volcanics

Name. Devils Playground Volcanics.

Derivation of name. Devils Playground, a playa on northeastern KINGOONYA 1:250 000 sheet, GDA94, zone 53, centred at 622000mE, 6679000mN.

Distribution. Central-northern KINGOONYA and central-southern BILLA KALINA 1:250 000 sheets, entirely subsurface, north and west of Millers Creek Homestead.

Type drillhole. DP1 (Esso Australia Ltd 1985), GDA94, zone 53, 581233mE, 6679463mN, 166.0–616.6 m (TD), cuttings 166.0–258.0 m, core 258.0–616.6 m.

Reference drillhole. Eromanga Uranium Limited BKDDH01, 601605mE, 6685192mN, zone 53, 421–599 m (TD).

Age and evidence. Late Archaean, ID-TIMS U–Pb zircon age 2558 ± 6 Ma on rhyodacite from DP1, sample 6037 RS31, 373.6–376.5 m.

Lithology. Green-grey basalt to andesite lava and breccia and lesser tuff; often porphyritic, locally amygdaloidal. Pink-grey rhyodacite lava and tuff, occasionally porphyritic or spherulitic, are intercalated in DP1. Greenschist-facies metamorphism, with development of biotite–actinolite–chlorite–epidote–albite–carbonate–titanate or sericite–chlorite–carbonate alteration and carbonate ± quartz veining. Moderate, but inhomogeneous foliation.

Thickness. Minimum width of 450.6 m intersected in DP1, with true minimum thickness somewhat less due to original layering recorded as dipping between 20 and 60 degrees.

Relationships and boundary criteria. Underlies Carboniferous–Permian Boorthanna Formation of the Arckaringa Basin. Relationship to remainder of the Mulgathing Complex or other units not exposed.

Province. Gawler Craton.

Parent. Mulgathing Complex.

Synonymy. Referred to informally as 'unnamed Archaean low-grade calcalkaline volcanics' or similar.

Comments. Although the Devils Playground playa is some distance from the area of occurrence of the Devils Playground Volcanics, the name is retained due to informal usage derived from the name of the exploration tenement under which DP1 was drilled. The unit is also interpreted in Eromanga Uranium BKDDH02, close to BKDDH01, and possibly in water bore Bertram Downs 2, 1.2 km north of DP1, this bore recovering hard green ?basic volcanic rock from 190.2–190.6 m.

Acknowledgements

Eromanga Uranium is acknowledged for discussions and for funding the geochemical data acquisition. Note that an attempt to separate zircons from PIRSA sample R1667143 was made at the Geoscience Australia mineral separation laboratory, however no zircon was recovered. Our understanding of the geology of these volcanics has benefitted from petrology reports by Alan Purvis of Pontifex and Associates. David Bruce collected the Sm–Nd isotopic data at the University of Adelaide. A helpful review by Massimo Raveggi is acknowledged.

References

Birt T and Reid AJ 2007. Archaean gold systems of South Australia. *MESA Journal* 46:29–33. Department of Primary Industries and Resources South Australia, Adelaide.

Cowley WM and Fanning CM 1991. Low-grade Archaean metavolcanics in the northern Gawler Craton. *Quarterly Geological Notes* 119:2–17. Geological Survey of South Australia.

Cowley WM and Martin AR 1991. *KINGOONYA, South Australia*, 1:250 000 Geological Series Explanatory Notes, sheet SH53-11. Department of Primary Industries and Resources South Australia, Adelaide.

Daly SJ and Fanning CM 1993. Archaean. In JF Drexel, WV Preiss and AJ Parker eds, *The geology of South Australia, Volume 1, The Precambrian*, Bulletin 54. Geological Survey of South Australia, Adelaide, pp. 32–49.

Daly SJ and van der Stelt BJ 1992. Archaean metabasic diamond drilling project, Open file Envelope 8541. Department of Primary Industries and Resources South Australia, Adelaide.

Esso Australia Ltd 1985. Devils Playground and Mount Eba, progress and final relinquishment reports for the period 13/3/80 to 28/3/86, Open file Envelope 3784. Department of Primary Industries and Resources South Australia, Adelaide.

Fanning CM, Reid A and Teale G 2007. *A geochronological framework for the Gawler Craton, South Australia*, Bulletin 55. Geological Survey of South Australia, Adelaide.

Fricke C 2005. Source and origin of the lower Gawler Range Volcanics (GRV), South Australia: geochemical constraints from mafic magmas. BSc thesis, Monash University, Melbourne.

Giles CW 1981. A comparative geochemical study of acid and basic volcanics from drillholes DP1, BD-1 and JD-1, Stuart Shelf, South Australia, Open file envelope 3784. Department of Primary Industries and Resources South Australia, Adelaide.

Hoatson DM, Sun S-S, Duggan MB, Davies MB, Daly SJ and Purvis AC 2005. Late Archaean Lake Harris Komatiite, central Gawler Craton, South Australia: geologic setting and geochemistry. *Economic Geology* 100:349–374.

Jagodzinski EA 2005. *Compilation of SHRIMP U-Pb geochronological data, Olympic Domain, Gawler Craton, South Australia, 2001-2003,* Record 2005/20. Geoscience Australia, Canberra.

Janoušek V, Farrow CM and Erban V 2006. Interpretation of whole-rock geochemical data in igneous geochemistry: introducing Geochemical Data Toolkit (GCDkit). *Journal of Petrology* 47:1255–1259.

Jensen LS 1976. A new cation plot for classifying subalkalic volcanic rocks. *Miscellaneous Paper* 66:1–21. Ontario Division of Mines.

McFarlane CRM, Mavrogenes JA and Tomkins AG 2007. Recognizing hydrothermal alteration through a granulite facies metamorphic overprint at the Challenger Au deposit, South Australia. *Chemical Geology* 243:64–89.

Pearce JA 1982. Trace element characteristics of lavas from destructive plate boundaries. In RS Thorpe ed., *Andesites*. Wiley, Chichester, pp. 525–548.

Plank T and Langmuir CH 1998. The chemical composition of subducting sediment and its consequences for the crust and mantle. *Chemical Geology* 145:325–394.

Reid AJ 2008. *Complete geochronology of the Gawler Craton, South Australia: 1970 to 2007,* Mineral Exploration Data Package 16. Department of Primary Industries and Resources South Australia, Adelaide.

Salters V and Stracke A 2004. Composition of the depleted mantle. *Geochemistry, Geophysics, Geosystems: doi:* 10.1029/2003GC000597.

Swain G, Woodhouse A, Hand M, Barovich K, Schwarz M and Fanning CM 2005. Provenance and tectonic development of the late Archaean Gawler Craton, Australia; U–Pb zircon, geochemical and Sm–Nd isotopic implications. *Precambrian Research* 141:106–136.

Taylor SR and McLennan SM 1985. *The continental crust: its composition and evolution.* Blackwell Scientific Publications.

Teale G, Brewer AM and Lynch JE 2006. Archaean and ?Palaeozoic base metal discoveries on the western Eyre Peninsula by Lynch Mining. *MESA Journal* 42:4–9.

Department of Primary Industries and Resources South Australia, Adelaide.

Thompson RN 1982. Magmatism of the British Tertiary volcanic province. *Scottish Journal of Geology* 18:49–107.

Wade B, Barovich K and Hand M 2006. Evidence for early Mesoproterozoic arc-related magmatism in the Musgrave Province, Australia. *Journal of Geology* 114:43–63.

Winchester JA and Floyd PA 1977. Geochemical discrimination of different magma series and their differentiation products using immobile elements. *Chemical Geology* 20:325–343.

For further information contact Anthony Reid, phone +61 8 8463 3039, email <Anthony.Reid@sa.gov.au>.

Large earthquakes south of Kangaroo Island

On 30 July 2009 a series of earthquakes began ~300 km south of Kangaroo Island (Fig. 1). On average, South Australia has only one magnitude 4 or greater event per year, yet in the space of three weeks this series south of Kangaroo Island produced five events between magnitude 4.0 and 4.5. The swarm occurred in a place where we have not recorded earthquakes before, well away from the continental slope, with no indication of a major transform fault.

Earthquakes occasionally occur along the continental shelf, but rarely in the deep ocean (apart from those along the mid-ocean ridge and associated crosscutting transform faults). It is assumed that the 1897 magnitude 6.5 event occurred on the continental shelf between Robe and Beachport (Fig. 1), but we have only the reports and intensity map to estimate the epicentre.

The 2009 July–August earthquake swarm shows a clear pattern in time, with outbursts at about six-day intervals, which may relate to tidal forces (Fig. 2). Most events under magnitude 3.2 would not have been detected.

Earthquakes along mid-ocean spreading zones are rarely large, although one of magnitude 7.1 did occur 1500 km SW of Adelaide in 2001. Where the crust is thin, as in most oceanic areas, it is considered that large ruptures cannot occur. Most earthquakes along the mid-ocean ridge are slip–strike, therefore posing no risk of tsunami. Larger events onshore are often thrust. These events were not large enough to calculate a mechanism.

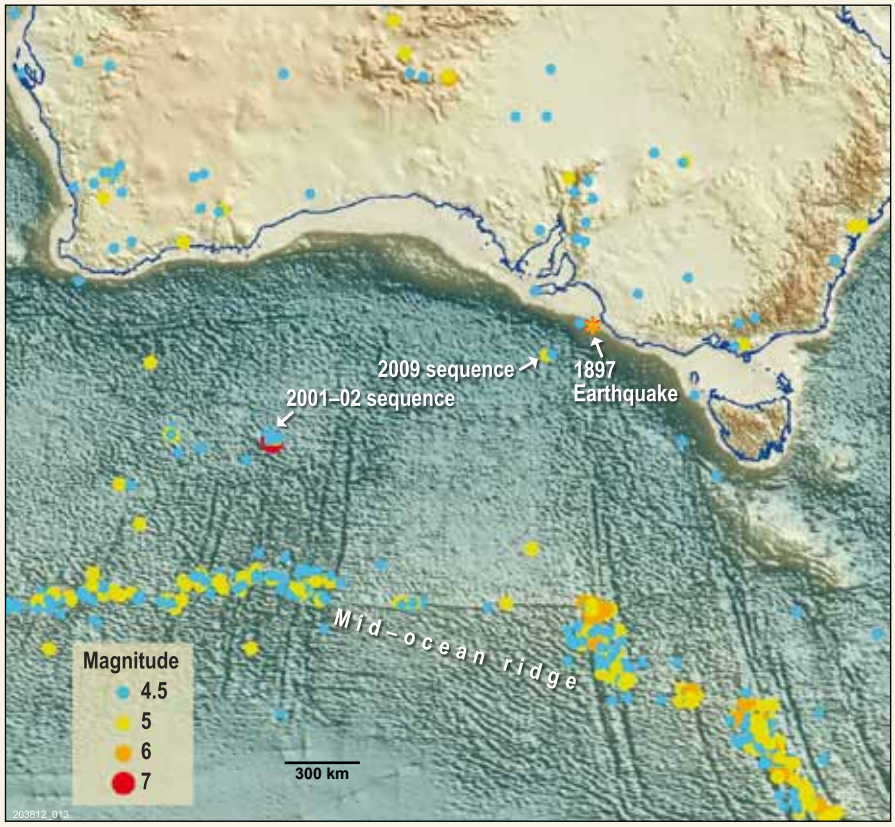

Figure 1 *Earthquakes 2001–09 (source: United States Geological Survey).*

For further information contact David Love, phone +61 8 8463 3177, email <David.Love@sa.gov.au>.

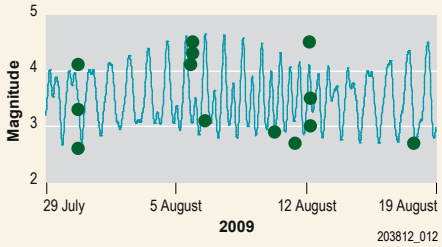

Figure 2 *Earthquakes (green dots) and Victor Harbor tides (blue line).*